

# Electric field driven stability control of skyrmions in an ultrathin transition-metal film

Souvik Paul\* and Stefan Heinze\*

*Institute of Theoretical Physics and Astrophysics, Christian-Albrechts-Universität zu Kiel,  
Leibnizstrasse 15, 24098 Kiel, Germany*

E-mail: paul@physik.uni-kiel.de; heinze@physik.uni-kiel.de

## Abstract

Using density functional theory (DFT), we study how the stability of individual magnetic skyrmions in an ultrathin transition-metal film can be controlled via the external electric fields. For applied electric fields of  $\mathcal{E} = \pm 0.5 \text{ V/\AA}$ , we find changes from 8 to 30% of the Heisenberg exchange, the Dzyaloshinskii-Moriya interaction, the magnetocrystalline anisotropy energy, and the higher-order exchange interactions. Based on atomistic spin simulations using the DFT parameters, we find that the energy barriers for electric field assisted skyrmion writing and deleting can vary by up to a factor of three more than the variations of the interactions. This unexpected result originates from the electric field induced shifts of the critical magnetic field, marking the onset of the field-polarized phase, which exhibits metastable skyrmions. The shift leads to an electric field dependent change of the skyrmion radius at a fixed magnetic field and explains the enhanced energy barrier variations.

## Keywords

Skyrmions, electric field effects, magnetic interactions, energy barriers

Magnetic skyrmions – topologically nontrivial swirling spin structures<sup>1,2</sup> – show great promises as information carriers in future magnetic memory and logic devices due to their nanoscale size and ultralow current-driven ma-

nipulation, achieved by spin transfer torque (STT)<sup>2-7</sup> and spin orbit torque.<sup>8-14</sup> The main drawback of these techniques to realize a low-energy-dissipation device is Joule heating, which destabilizes the skyrmionic bits. The electric field induced manipulation offers an efficient route for creating, deleting and controlling skyrmions avoiding the heating problem. The energy dissipation can be reduced by a factor of 100 by using the electric field as compared to STT.<sup>15</sup> Another important benefit of using an electric field is that it does not displace the skyrmionic bits, which is desirable for encoding information at a particular position.

In spite of recognizing the potential of electric field induced manipulation, only a few experimental studies have been reported on electric field induced switching of skyrmions and skyrmion bubbles in transition-metal multilayers<sup>16-19</sup> and recently in multiferroic heterostructures.<sup>20,21</sup> Theoretical studies have addressed either the variation of magnetic anisotropy<sup>22-24</sup> or the Dzyaloshinskii-Moriya interaction (DMI)<sup>19,25</sup> either directly with electric field or indirectly due to electric field induced strain.<sup>20,21</sup> However, it is the interplay of the exchange interaction, the DMI, and the anisotropy which is responsible for the properties of magnetic skyrmions.<sup>1</sup> Therefore, in a study for the influence of the electric field, one needs to take the variation of all these interactions into account. Moreover, the importance of higher-order exchange interactions (HOI) beyond the conventional Heisenberg pair-wise

exchange mechanism in ultrathin films for the stability of skyrmions has recently been demonstrated.<sup>26</sup>

Here, we study the stability of isolated magnetic skyrmions in an ultrathin film from first-principles electronic structure theory. For the model system of an atomic Fe/Rh bilayer on the Re(0001) surface, we find from DFT calculations that the pair-wise exchange varies by about 15%, the DMI by only 8%, while the magnetocrystalline anisotropy energy (MAE) varies by about 30% for an electric field difference of 1 V/Å. Among the HOI, only the four-site four spin interaction shows a significant variation of about 22% for an electric field difference of 1 V/Å. We study the formation and collapse of skyrmions under the electric fields by atomistic spin simulations using the DFT parameters. The energy barriers preventing the collapse of individual skyrmions varies by about 60% and the barriers for skyrmion creation by about 30% for an electric field difference of 1 V/Å. The enhanced energy barriers with respect to the variation of the magnetic interactions can be explained by a shift of the critical magnetic field by about 0.6 T of the phase boundary between the skyrmion and field-polarized state. Thereby, the skyrmion radius varies significantly with electric field at a given magnetic field value which leads to the large change of the energy barriers.

Figure 1a shows the setup used for the DFT calculations performed via the FLEUR code<sup>28</sup> (see methods for computational details). The electric field is introduced by placing a charged sheet in the vacuum region of Fe/Rh/Re(0001) film.<sup>29</sup> The charge neutrality of the whole system is maintained by adding or removing the same amount of opposite charge to the film. In this way, a uniform electric field perpendicular to the film surface is generated. For the electric field strength, we chose values of  $\mathcal{E} = \pm 0.5$  V/Å in agreement with the experimental work in Ref.,<sup>16</sup> which demonstrated switching of skyrmions in Fe films at these electric fields.

We first discuss the energy dispersion  $E(\mathbf{q})$  of homogeneous flat spin spirals without spin-orbit coupling (SOC) obtained via DFT for

Fe/Rh/Re(0001) along two high-symmetric directions of the two-dimensional Brillouin zone (2DBZ) (Figure 1b). The magnetic moment  $\mathbf{M}_i$  at lattice site  $\mathbf{R}_i$  in a spin spiral is given by  $\mathbf{M}_i = M(\cos \mathbf{q}\mathbf{R}_i, \sin \mathbf{q}\mathbf{R}_i, 0)$ , where  $M$  is the size of the moment and  $\mathbf{q}$  is the spin spiral vector. At  $\mathcal{E} = 0$ , the ferromagnetic (FM) state ( $\bar{\Gamma}$  point) is energetically lowest. The Néel state with an angle of 120° between adjacent spins ( $\bar{K}$  point) and the row-wise antiferromagnetic (AFM) state ( $\bar{M}$  point) are significantly higher in energy (Figure 1b). The dispersion calculated for  $\mathcal{E} = \pm 0.5$  V/Å shows the same trend as of the zero field. The electric field induced modification of  $E(\mathbf{q})$  is not visible on this scale at small  $\mathbf{q}$  (see Figure S2 for a close-up), however, it is significant at large  $\mathbf{q}$  with an energy rise (drop) at  $\mathcal{E} > 0$  ( $\mathcal{E} < 0$ ). The magnetic moment of Fe is about 2.9  $\mu_B$ , which does not change much with  $\mathcal{E}$  and remains fairly constant upon varying  $\mathbf{q}$  (Figure S3). The local density of states shows that the main effect of the spin-dependent screening of the electric field occurs in the Fe and Rh layer, while the Re layer is affected very weakly (Figure S4).

SOC adds two contributions: the MAE and the DMI (inset of Figure 1b). The easy magnetization axis of the Fe/Rh bilayer is in the film plane and the value of the MAE is  $K = -0.2$  meV/Fe atom that leads to an energy offset of  $K/2$  for spin spirals with respect to the FM state ( $\bar{\Gamma}$  point). The MAE changes only slightly upon applying an electric field barely visible in the inset. The DMI arises due to breaking of the inversion symmetry at the surface and here favors cycloidal spin spirals with a clockwise rotational sense (inset of Figure 1b). For  $\mathcal{E} = +0.5$  V/Å, the spin spiral energy minimum is at  $-0.05$  meV/Fe with respect to the FM state and the spiral exhibits a pitch of 18.4 nm. For  $\mathcal{E} = -0.5$  V/Å, the minimum is lower at an energy of  $-0.20$  meV/Fe and the pitch significantly decreases to 10.2 nm. The field-induced change of the energy minimum by 0.15 meV/Fe atom is significant since the Zeeman energy due to an applied magnetic field of 1 T amounts to about 0.2 meV/Fe atom.

Since the HOI beyond pair-wise Heisenberg type exchange can be important in transition-

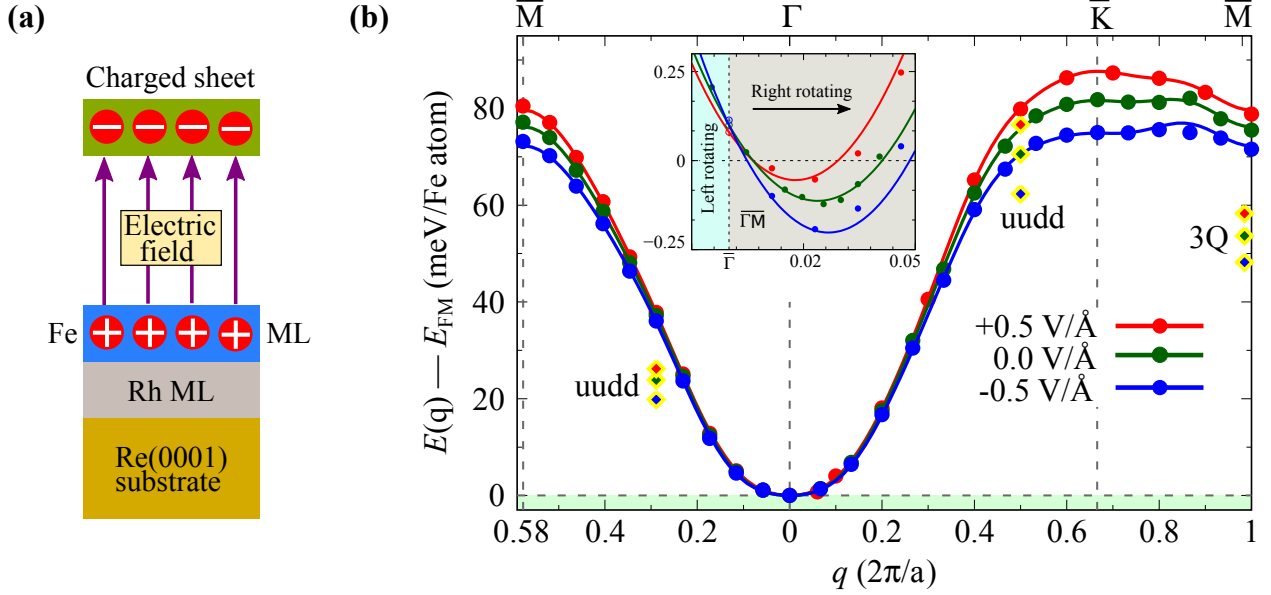


Figure 1: (a) Illustration of the Fe monolayer (ML) on a Rh ML on the Re(0001) surface, denoted as Fe/Rh/Re(0001), exposed to a perpendicular uniform electric field. In the DFT calculation, the electric field is created by a charged sheet located at 5.3 Å above the Fe layer. (b) Energy dispersion  $E(\mathbf{q})$  of flat spin spirals along two high symmetry directions ( $\bar{\Gamma}\bar{K}\bar{M}$  and  $\bar{\Gamma}\bar{M}$ ) without SOC at  $\mathcal{E} = +0.5$  V/Å (red),  $0.0$  V/Å (green)<sup>27</sup> and  $-0.5$  V/Å (blue). The filled circles represent DFT data and the solid lines are fit to the Heisenberg model. The filled diamonds represent the multi- $Q$  ( $3Q$  and  $uudd$ ) states without SOC, which are shown at the  $\mathbf{q}$  points of the corresponding single- $Q$  states (Figure S1 for spin structures). Inset shows  $E(\mathbf{q})$  of flat cycloidal spin spirals including DMI and MAE along  $\bar{\Gamma}\bar{M}$  for the three electric field values. The filled circles represent DFT data and the solid lines are fits to the Heisenberg plus DMI spin model. Grey (cyan) shaded region indicates right (left) rotating spin spirals. Note that the MAE shifts  $E(\mathbf{q})$  by  $K/2$  with respect to the FM state.

metal films<sup>30–35</sup> and for skyrmions,<sup>26,36</sup> we have also calculated their variation upon applying electric fields. To calculate the biquadratic interaction as well as the three-site and the four-site four spin interactions,<sup>34</sup> we consider three multi- $Q$  states: the two collinear up-up-down-down ( $uudd$ ) states<sup>37</sup> and a three-dimensional noncollinear  $3Q$ -state<sup>30</sup> (see supporting information for details). As seen in Figure 1b, the multi- $Q$  states, calculated at zero and finite electric fields, are lower in energy compared to the corresponding spin spiral states (for energy differences see table S2). The energies of the multi- $Q$  states shift with field in a similar way as the energy dispersion, i.e., their energy increases (decreases) for positive (negative) electric field.

The total energy from DFT calculations are

used to parametrize an atomistic spin model which is given by:

$$\begin{aligned}
\mathcal{H} = & - \sum_{\langle ij \rangle} J_{ij} (\mathbf{m}_i \cdot \mathbf{m}_j) - \sum_{\langle ij \rangle} \mathbf{D}_{ij} \cdot (\mathbf{m}_i \times \mathbf{m}_j) \\
& - \sum_i K (m_i^z)^2 - \sum_i \mu_s \mathbf{B} \cdot \mathbf{m}_i - B_1 \sum_{\langle ij \rangle} (\mathbf{m}_i \cdot \mathbf{m}_j)^2 \\
& - 2 Y_1 \sum_{\langle ijk \rangle} (\mathbf{m}_i \cdot \mathbf{m}_j) (\mathbf{m}_j \cdot \mathbf{m}_k) \\
& - K_1 \sum_{\langle ijkl \rangle} (\mathbf{m}_i \cdot \mathbf{m}_j) (\mathbf{m}_k \cdot \mathbf{m}_l) + (\mathbf{m}_i \cdot \mathbf{m}_l) (\mathbf{m}_j \cdot \mathbf{m}_k) \\
& - (\mathbf{m}_i \cdot \mathbf{m}_k) (\mathbf{m}_j \cdot \mathbf{m}_l) \quad (1)
\end{aligned}$$

where the magnetic moment of Fe at site  $i$  is denoted by  $\mathbf{M}_i$  and  $\mathbf{m}_i = \mathbf{M}_i/M_i$ .  $J_{ij}$ ,  $\mathbf{D}_{ij}$ ,  $\mu_s$  and  $K$  denote the pair-wise exchange constants, the DMI vectors, the magnetic moment

Table 1: Exchange constants for  $i$ -th nearest-neighbors ( $J_i$ ), biquadratic exchange constant ( $B_1$ ), three-site four spin exchange constant ( $Y_1$ ), four-site four spin exchange constant ( $K_1$ ), effective DMI constant ( $D_{\text{eff}}$ ), and the MAE constant ( $K$ ) for Fe/Rh/Re(0001) at three electric field values. The positive sign of  $D_{\text{eff}}$  indicates a preferred clockwise rotational sense and negative value of  $K$  indicates an in-plane easy magnetization axis. Data of  $\mathcal{E}= 0.0 \text{ V/\AA}$  are taken from Ref.<sup>26</sup> All energies are given in meV.

| Electric field       | $J_1$ | $J_2$ | $J_3$ | $J_4$ | $J_5$ | $J_6$ | $J_7$ | $B_1$ | $Y_1$ | $K_1$ | $D_{\text{eff}}$ | $K$   |
|----------------------|-------|-------|-------|-------|-------|-------|-------|-------|-------|-------|------------------|-------|
| +0.5 V/ $\text{\AA}$ | 9.37  | -1.03 | 0.07  | -0.24 | 0.27  | -0.01 | -0.12 | -0.34 | 1.05  | -1.23 | 0.87             | -0.16 |
| 0.0 V/ $\text{\AA}$  | 8.85  | -0.77 | -0.05 | -0.22 | 0.27  | 0.05  | -0.16 | -0.39 | 1.00  | -1.36 | 0.89             | -0.20 |
| -0.5 V/ $\text{\AA}$ | 8.08  | -0.55 | 0.03  | -0.20 | 0.23  | 0.01  | -0.12 | -0.33 | 1.00  | -1.53 | 0.94             | -0.22 |

and the MAE constant, respectively.  $B_1$  is the biquadratic constant,  $Y_1$  and  $K_1$  are the three-site and four-site four spin constant, respectively. The higher-order interactions are taken into account in nearest-neighbor approximation since they arise from fourth-order perturbation theory.<sup>34</sup>

The DFT values of the interaction parameters are given in table 1 for the three considered  $\mathcal{E}$  strengths. At  $\mathcal{E}= +0.5 \text{ V/\AA}$ , the ferromagnetic nearest-neighbor exchange constant,  $J_1$ , is enhanced by about 6%, while at  $\mathcal{E}= -0.5 \text{ V/\AA}$ , it decreases by about 9% with respect to zero  $\mathcal{E}$ . The absolute change of  $J_1$  amounts to about 1.3 meV for a field change by 1 V/ $\text{\AA}$ , which is similar to the value of 1.2 meV, reported from a DFT study for a Co monolayer (ML) on Pt(111).<sup>38</sup>  $J_2$  becomes more (less) antiferromagnetic at  $\mathcal{E} > 0$  ( $\mathcal{E} < 0$ ) with a variation almost linear with field. The pair-wise exchange constants beyond second neighbors remain fairly constant with electric fields. Among the HOI, only the four-site four spin interaction,  $K_1$ , varies significantly with electric fields. It shows a decrease of about 10% at  $\mathcal{E}= +0.5 \text{ V/\AA}$  and an increase of about 13% at  $\mathcal{E}= -0.5 \text{ V/\AA}$ .

The effective nearest-neighbor DMI constant,  $D_{\text{eff}}$ , varies by only 0.07 meV upon changing  $\mathcal{E}$  by 1 V/ $\text{\AA}$ , which amounts to a relative change of  $\Delta D_1/D_1 \approx 0.08$ . Since the Re layer with a large SOC constant is already screened by the electric field, it exhibits only a small change (Figure S5). A large effect is observed for the Rh layer as it is closer to the surface, however, its contribution to the total DMI is small. The

field-induced variation of the DMI is still twice larger than the previously reported value for a MgO/Co/Pt trilayer.<sup>25</sup> The MAE changes by 30% from  $\mathcal{E}= +0.5 \text{ V/\AA}$  to  $\mathcal{E}= -0.5 \text{ V/\AA}$  and it contributes 0.03 meV to the change of the spin spiral energy minimum (Figure 1b).

Summarizing the DFT results, we find that the electric field influences the ground state through a variation of DMI, exchange interactions and MAE, which leads to the change of the spin spiral period and the depth of the energy minimum.

Next we show by atomistic spin simulations based on Eq. (1) with the DFT parameters that the field-dependent spin spiral minimum allows to tune the onset of the FM phase, where magnetic skyrmions are metastable. From the zero-temperature phase diagram (Figure 2), we find that, independent of  $\mathcal{E}$ , a spin spiral ground state occurs at zero and small magnetic fields, consistent with the spin spiral minima in Figure 1b. At  $B > 0.7 \text{ T}$ , the skyrmion lattice phase becomes energetically favorable. With further increase of the magnetic field, the field-polarized (FM) phase becomes the lowest energy state. Note that the onset of the FM phase, i.e., the critical field  $B_c$ , changes with  $\mathcal{E}$  (inset of Figure 2c). The change of  $B_c$  (0.56 T) with electric field (1 V/ $\text{\AA}$ ) is close to the estimated value from the spin spiral energy minimum in Figure 1b ( $\approx 0.75 \text{ T}$ ).

Now we consider individual magnetic skyrmions. We find that the skyrmion radius increases significantly for  $\mathcal{E} < 0$ , while it decreases for  $\mathcal{E} > 0$  (Figure 3a). At first sight,

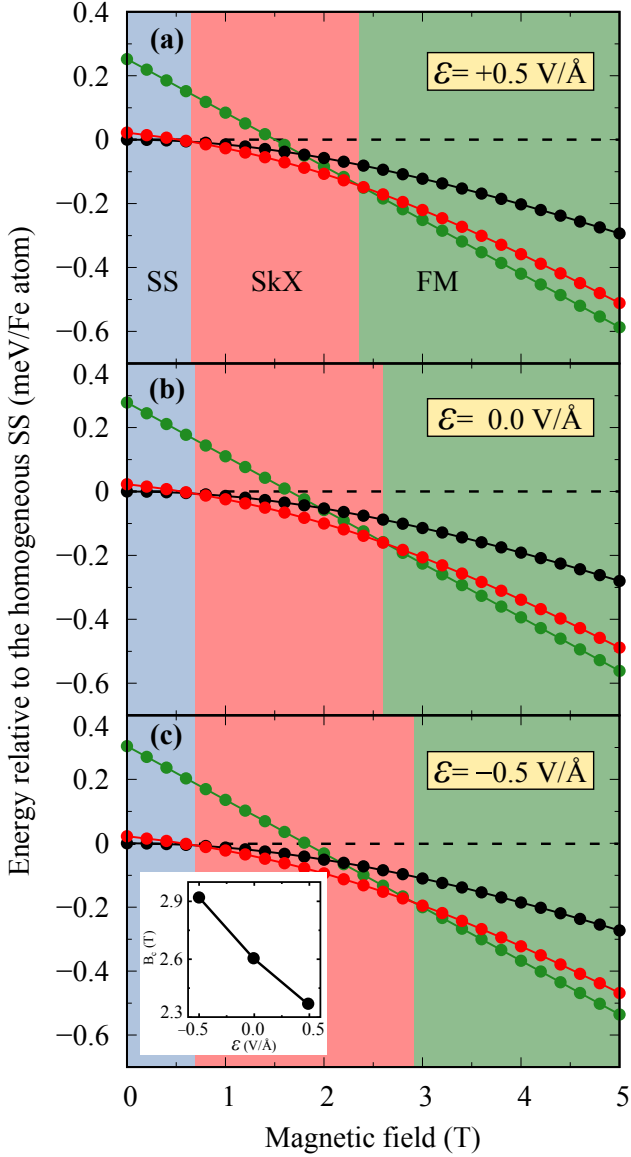


Figure 2: Zero temperature phase diagram of Fe/Rh/Re(0001) at (a)  $\mathcal{E} = +0.5 \text{ V/\AA}$  (b)  $\mathcal{E} = 0 \text{ V/\AA}$  and (c)  $\mathcal{E} = -0.5 \text{ V/\AA}$ . Energies of the relaxed spin spiral (SS, black circles), skyrmion lattice (SkX, red circles) and field-polarized ferromagnetic (FM, green circles) states are shown with reference to the homogeneous spin spiral (dashed line). The SS, SkX and FM phases are denoted with blue, red and green background colors, respectively. Inset of (c) shows the variation of the critical field  $B_c$  (onset of FM phase) with  $\mathcal{E}$ .

it seems surprising that the order of skyrmion radius with  $\mathcal{E}$  is reversed with respect to the change of the spin spiral period at the energy minimum found from DFT (Figure 1b). How-

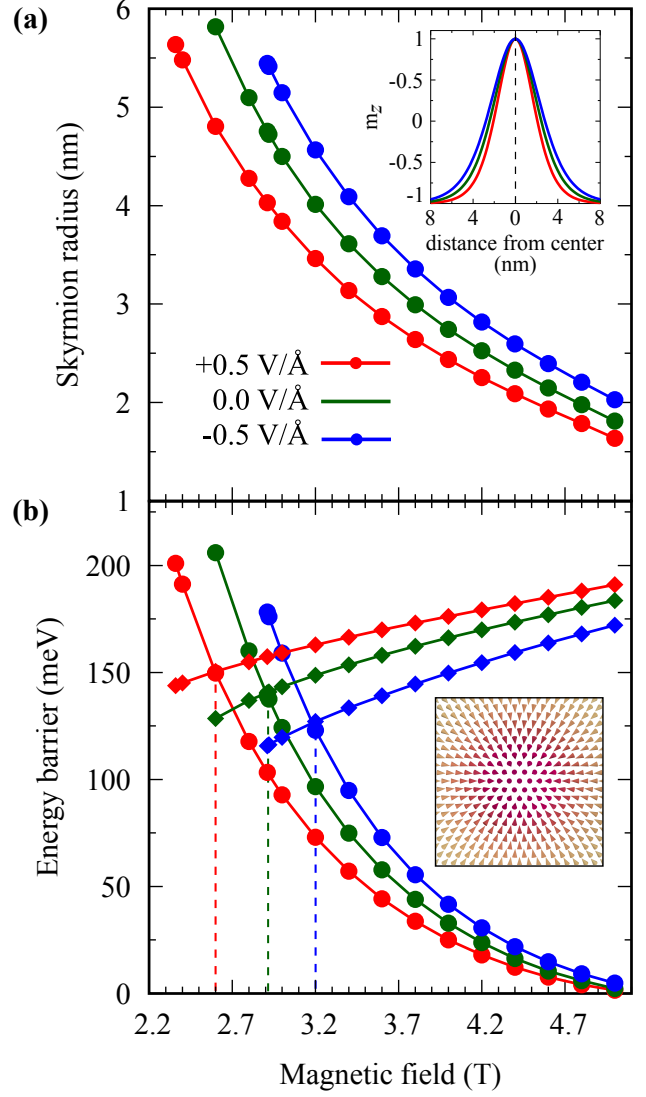


Figure 3: (a) Radius and (b) energy barriers of isolated skyrmions with applied magnetic fields at  $\mathcal{E} = +0.5 \text{ V/\AA}$  (red),  $\mathcal{E} = 0 \text{ V/\AA}$  (green) and  $\mathcal{E} = -0.5 \text{ V/\AA}$  (blue). In (b), filled circles show collapse barriers,  $\Delta E_{\text{col}}$ , while filled diamonds mark creation barriers,  $\Delta E_{\text{crea}}$ . Inset of (a) shows the skyrmion profiles at  $B = 3 \text{ T}$  for three values of  $\mathcal{E}$  and (b) shows the skyrmion spin structure for  $\mathcal{E} = 0 \text{ V/\AA}$  at  $B = 3 \text{ T}$ .

ever, this is due to the fact that the critical magnetic field at which the transition from the skyrmion to the field-polarized (FM) phase occurs also changes with  $\mathcal{E}$ . Since, in an experiment, switching of a skyrmion is performed at a fixed magnetic field,<sup>16,39</sup> the variation of the skyrmion radius (see inset of Figure 3a) strongly affects the energy barriers for skyrmion creation or annihilation as shown below.<sup>40</sup>

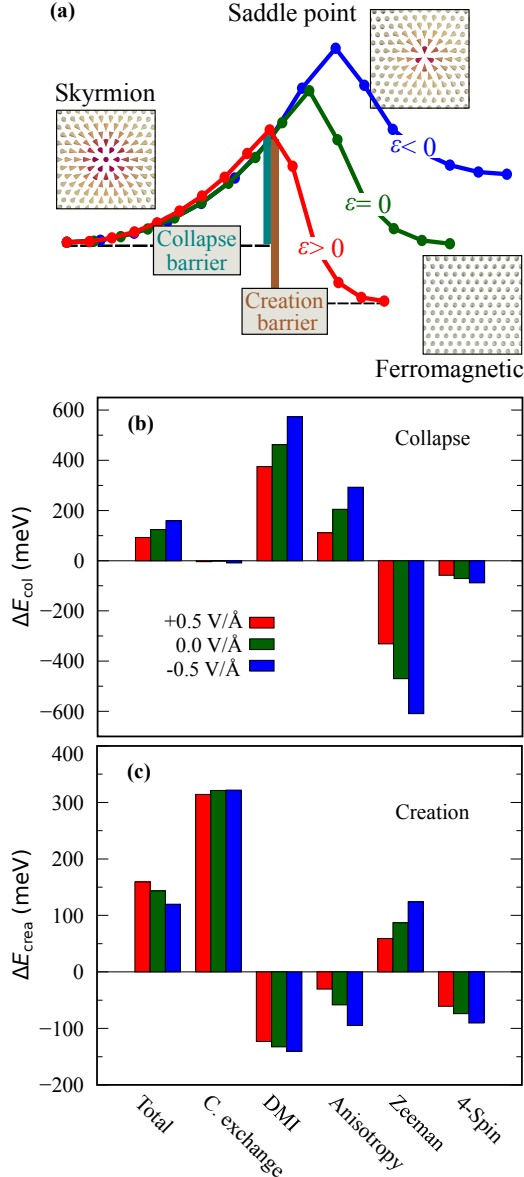


Figure 4: (a) Minimum energy paths (MEP) from the initial (skyrmion) to the final (FM) state at  $B = 3$  T for the three electric fields. The energy difference between the saddle point and the skyrmion (FM) state defines the collapse (creation) barrier. Total and individual energy contributions at  $B = 3$  T for (b) the collapse barrier and (c) for the creation barrier. For energy decomposition of the full MEP see Figure S6. Combined exchange (C. exchange) indicates the sum of pair-wise exchange, bi-quadratic and three-site four spin interactions. The four-site four spin interaction is denoted as 4-Spin for brevity. The electric field  $\mathcal{E} = +0.5$  V/Å  $0$  V/Å and  $-0.5$  V/Å are shown as red, green and blue, respectively.

We used the geodesic nudged elastic band (GNEB) method<sup>41</sup> to calculate the minimum energy path (MEP) between an isolated skyrmion and the FM background. The skyrmions annihilate by the well-known radial collapse mechanism.<sup>42</sup> From MEP, we find the energy barrier  $\Delta E_{\text{col}}$  protecting the skyrmion from collapsing into the FM state, i.e., the difference between the saddle point (SP), maximum energy point on the path, and the initial (skyrmion) state (Figure 4a). The creation barrier,  $\Delta E_{\text{crea}}$ , is obtained from the difference between the SP and the final (FM) state.

It is apparent that  $\Delta E_{\text{col}}$  decreases as a function of applied magnetic field similar to the decrease of the skyrmion radius (Figure 3b). This is due to the fact that the energy terms which contribute to the barrier, in particular the DMI, scale with the number of spins in the skyrmion. On the other hand,  $\Delta E_{\text{crea}}$  displays only a small nearly linear rise with applied magnetic field (Figure 3b). This can be understood from the fact that it depends on the energy difference of the FM state and the saddle point. We can relate  $\Delta E_{\text{crea}}$  to the energy difference between the skyrmion and the FM state,  $\Delta E_{\text{sk-FM}}$ , and the collapse barrier by  $\Delta E_{\text{crea}} = \Delta E_{\text{sk-FM}} + \Delta E_{\text{col}}$  (Figure 4a). As discussed above,  $\Delta E_{\text{col}}$  decreases with  $B$ . However, the FM state becomes more favorable with increasing magnetic field and  $\Delta E_{\text{sk-FM}}$  increases (Figure 2). The gradual rise of  $\Delta E_{\text{crea}}$  with magnetic field is due to these two opposing contributions.

The magnetic field at which both barriers are equal (green curve in Figure 4a) marks the transition from the skyrmion to the FM phase. As seen in the phase diagrams (Figure 2), this critical magnetic field shifts with  $\mathcal{E}$ . At  $\mathcal{E} = 0$  V/Å,  $B_c$  is about 2.9 T. If one changes the electric field to  $+0.5$  V/Å, at a fixed magnetic field, the creation barrier is enhanced while the collapse barrier decreases since  $B_c$  shifts to a lower value (Figure 2a). Therefore, the FM state becomes more favorable (red curve in Figure 4a). For  $\mathcal{E} < 0$ , the opposite effect occurs since one moves into the skyrmion phase at a fixed magnetic field of 2.9 T. The skyrmion state is therefore lower (blue curve in Figure 4a) than the FM state and the collapse barrier rises. This ex-

plains why collapse and creation barriers show opposite trends upon variation of the electric field.

Now we quantify the energy barrier at  $B=3$  T in terms of the magnetic interactions (Figure 4b,c). At this value, we find  $\Delta E_{\text{col}} \approx 125$  meV for zero electric field.  $\Delta E_{\text{col}}$  increases by  $\approx 35$  meV at  $\mathcal{E} = -0.5$  V/Å (Figure 4b). Interestingly, the total energy barrier arises due to the increase of DMI ( $\approx 110$  meV) and the MAE ( $\approx 90$  meV), while both the Zeeman term ( $\approx -140$  meV) and the four-site four spin interaction ( $\approx -20$  meV) lead to opposite contributions and thus reducing the electric field effect.<sup>43</sup> The combined exchange interaction, i.e., the sum of the contributions from pair-wise exchange, biquadratic and three-site four spin interaction, does not contribute to the change of energy barriers. For  $\mathcal{E} = +0.5$  V/Å, we find a decrease of  $\Delta E_{\text{col}}$  by  $\approx 35$  meV and the different interactions contribute in an analogous way.

The variation of  $\Delta E_{\text{col}}$  by about  $\pm 30\%$  for  $\mathcal{E} = \pm 0.5$  V/Å cannot be directly understood from the electric field induced changes of the magnetic interactions. The magnetic moment does not change with  $\mathcal{E}$ . Thus the variation of the Zeeman energy must be directly linked to the change of the skyrmion radius with  $\mathcal{E}$  (Figure 3). For  $\mathcal{E} = \pm 0.5$  V/Å, the skyrmion radius varies by 1.3 nm at  $B=3$  T. We can estimate the relative change of the number of moments in the skyrmion from  $\Delta N_{\text{sk}}/N_{\text{sk}} = (R_{\text{sk}}^2(\mathcal{E}) - R_{\text{sk}}^2(0))/R_{\text{sk}}^2(0) \approx 0.3$  which closely matches the variation of the Zeeman contribution to the energy barrier  $\Delta E_{\text{Zeeman}}/E_{\text{Zeeman}} \approx 0.3$ . The electric field dependent skyrmion radius also explains the large relative change of the DMI term,  $\Delta E_{\text{DMI}}/E_{\text{DMI}} \approx 0.25$ , and the anisotropy term,  $\Delta E_{\text{MAE}}/E_{\text{MAE}} \approx 0.45$  which are about four times larger than the change of  $D_{\text{eff}}$  and  $K$ , respectively (table 1). For the four-spin interaction,  $K_1$ , this effect is much reduced since the barrier contribution of this term depends on the saddle point structure<sup>26</sup> which is less affected by the electric field.

The creation barrier (Figure 4c) varies by about 15% for  $\mathcal{E} = \pm 0.5$  V/Å, but displays an opposite trend with respect to  $\Delta E_{\text{col}}$ , i.e., the barrier decreases for  $\mathcal{E} < 0$  and rises for  $\mathcal{E} > 0$ .

As stated above, this can be explained based on MEM (Figure 4a). The energy decomposition (Figure 4c) shows that the DMI plays a minor role while MAE and four-spin exchange determine the electric field dependence.<sup>44</sup> The Zeeman term shows an opposite trend and again reduces the electric field effect. The scaling of anisotropy and Zeeman term with  $\mathcal{E}$  is also much larger than expected from the electric field induced changes of the magnetic interactions and is due to the change of skyrmion radius as for  $\Delta E_{\text{col}}$ .

We can estimate the field-induced variation of skyrmion lifetime from the Arrhenius law  $\tau = \tau_0 \exp(\Delta E_{\text{col}}/k_{\text{B}}T)$ . If we neglect the variation of the attempt frequency  $\tau_0$ , the ratio of lifetimes at  $B=3$  T is given by  $\tau(\mathcal{E} = +0.5 \text{ V/Å})/\tau(\mathcal{E} = 0) = \exp(-35 \text{ meV}/k_{\text{B}}T)$ . This would lead to a change of the skyrmion lifetime by a factor of about  $2 \times 10^{-4}$  at a temperature of  $T = 50$  K, which is the estimated effective temperature due to the electric current in a scanning tunneling microscopy experiment.<sup>42,45</sup> Therefore, a significant effect in deleting individual skyrmions can be obtained by a local electric field in the tunnel junction. A similar estimate for the creation leads to a factor of  $8 \times 10^{-3}$ .

We have demonstrated that the stability of isolated skyrmions in an ultrathin film can be varied significantly by external electric fields. Based on DFT, we show that all relevant magnetic interactions are modified. These electric field induced changes lead to a shift of the critical magnetic field for the onset of the field-polarized phase, which exhibits metastable skyrmions. Therefore, creation and collapse barriers are much larger than expected from the variations of the interactions. Our study shows that it is indispensable to consider all magnetic interactions to evaluate the electric-field effect on skyrmion stability.

## Methods

**First-principles calculations** All calculations with electric field were performed using the FLEUR code.<sup>28</sup> We relaxed the top three lay-



ers of Fe/Rh/Re(0001), i.e., the Fe and Rh layers and the first Re layer along the  $z$ -direction by minimizing the atomic force on each atoms by less than 0.04 eV/Å in the presence of  $\mathcal{E} = \pm 0.5$  V/Å. We chose the generalized gradient approximation (GGA) exchange-correlation (XC) functional as parametrized by Perdew, Burke and Ernzerhof,<sup>46</sup> 66  $k$  points in 2DBZ and  $k_{max} = 4.0$  a.u.<sup>-1</sup> for relaxation. We find that there were almost no changes (up to second decimal place) of the top three inter-layer distances as compared to the zero field values given in Ref.<sup>27</sup> Therefore, we take the same interlayer distances as in Ref.<sup>27</sup> Similar to our result, no electric field induced relaxation was observed in a Co ML on the Pt(111) surface.<sup>38</sup>

To check the existence of a noncollinear ground state and to extract the Heisenberg pair-wise exchange parameters, we calculated the energy dispersion of homogeneous flat spin spirals, which are characterized by a wave vector  $\mathbf{q}$  in 2DBZ and an angle  $\phi = \mathbf{q} \cdot \mathbf{R}$  between adjacent magnetic moments separated by lattice vector  $\mathbf{R}$ .<sup>47</sup> We used the generalized Bloch theorem<sup>48</sup> to compute spin spiral energies within the chemical unit cell. To study the surface, we chose an asymmetric film of two atomic overlayers on nine Re substrate layers. Since we used an asymmetric film to compute the magnetic interactions and our interest is on the electric field induced changes in magnetism, we only apply an electric field perpendicular to the Fe surface. To be consistent with the zero electric field spin spiral calculations, we used the local density approximation (LDA) XC functional form given by Vosko, Wilk and Nusair,<sup>49</sup> a dense mesh of  $44 \times 44$   $k$ -points in the full 2DBZ and  $k_{max} = 4.0$  a.u.<sup>-1</sup>.

The DMI was computed within the first-order perturbation theory<sup>50</sup> on the self-consistent spin spiral state. The MAE was calculated within the second variation approach on a self-consistent scalar-relativistic density. To obtain an accurate value of the MAE, we have varied the substrate layers from 13 to 17 of the asymmetric film.

Due to the large 2D unit cell, the energy of the multi- $Q$  states were evaluated from asymmetric films consisting of 8 layers in total. However,

we have checked for zero electric field that the energy differences between the 8 and 11 layer film calculations is less than 1 meV.

**Atomistic spin dynamics simulations** We relaxed the spin spirals, skyrmion lattice and isolated skyrmions using the Landau-Lifshitz equation, which is a combination of the precession and the damping terms, respectively, as given below:

$$\hbar \frac{d\mathbf{m}_i}{dt} = \frac{\partial H}{\partial \mathbf{m}_i} \times \mathbf{m}_i - \alpha \left( \frac{\partial H}{\partial \mathbf{m}_i} \times \mathbf{m}_i \right) \times \mathbf{m}_i \quad (2)$$

where  $\hbar$  is the reduced Planck constant,  $\alpha$  is the damping parameter and the Hamiltonian  $H$  is defined in Eq. (1). We used a time step of 0.1 fs,  $\alpha$  is varied from 0.05 to 0.1 and the simulations were carried out over 4 to 6 million steps for relaxation. We solve the equation by semi-implicit method as proposed by Mentink *et al.*<sup>51</sup>

**Geodesic nudged elastic band method** We first create the isolated skyrmions in the field-polarized background, i.e., at a magnetic field above  $B_c$  from the theoretical profile<sup>1</sup> and then relax the spin structure using spin dynamics with the full set of DFT parameters (table 1 and table S1). We computed the collapse and creation barriers of isolated skyrmions using the GNEB method.<sup>52</sup> The method calculates the MEP connecting the initial state (IS), i.e., skyrmions and final state (FS), FM state, on a multidimensional energy surface. Within GNEB, an initial path connecting the IS and FS is created by a chain of images of the system. The objective of the method is to bring the initial path to MEP via relaxing the intermediate images. The relaxation is achieved by a force projection scheme. For this, the effective field is calculated at each image and its local tangent to the path is replaced by a spring force which maintains a uniform distribution of images. The maximum energy of MEP corresponds to the saddle point (SP) which defines the energy barrier separating two stable states. We compute the energy of the SP more accurately using a climbing image (CI) method on



top of GNEB.

### Acknowledgement

We gratefully acknowledge computing time at the supercomputer of the North-German Supercomputing Alliance (HLRN) and financial support from the Deutsche Forschungsgemeinschaft (DFG, German Research Foundation) via project no. 414321830 (HE3292/11-1).

## References

- (1) Bogdanov, A. N.; Hubert, A. *phys. stat. sol. (b)* **1994**, *186*, 527–543.
- (2) Nagaosa, N.; Tokura, Y. *Nat. Nanotechnol.* **2013**, *8*, 899–911.
- (3) Tomasello, R.; Martinez, E.; Zivieri, R.; Torres, L.; Carpentieri, M.; Finocchio, G. *Sci. Rep.* **2014**, *4*, 6784.
- (4) Zhou, Y.; Ezawa, M. *Nat. Commun.* **2014**, *5*, 4652.
- (5) Iwasaki, J.; Mochizuki, M.; Nagaosa, N. *Nat. Commun.* **2013**, *4*, 1463.
- (6) Sampaio, J.; Cros, V.; Rohart, S.; Thiaville, A.; Fert, A. *Nat. Nanotechnol.* **2013**, *8*, 839–844.
- (7) Fert, A.; Cros, V.; Sampaio, J. *Nat. Nanotechnol.* **2013**, *8*, 152–156.
- (8) Chernyshov, A.; Overby, M.; Liu, X.; Furdyna, J. K.; Lyanda-Geller, Y.; Rokhinson, L. P. *Nat. Phys.* **2009**, *5*, 656 – 659.
- (9) Miron, I. M.; Gaudin, G.; Auffret, S.; Rodmacq, B.; Schuhl, A.; Pizzini, S.; Vogel, J.; Gambardella, P. *Nat. Mater.* **2010**, *9*, 230 – 234.
- (10) Miron, I. M.; Garello, K.; Gaudin, G.; Zermatten, P.-J.; Costache, M. V.; Auffret, S.; Bandiera, S.; Rodmacq, B.; Schuhl, A.; Gambardella, P. *Nature* **2011**, *476*, 189 – 193.
- (11) Liu, L.; Pai, C.-F.; Li, Y.; Tseng, H. W.; Ralph, D. C.; Buhrman, R. A. *Science* **2012**, *336*, 555 – 558.
- (12) Woo, S.; Song, K. M.; Han, H.-S.; Jung, M.-S.; Im, M.-Y.; Lee, K.-S.; Song, K. S.; Fischer, P.; Hong, J.-I.; Choi, J. W.; Min, B.-C.; Koo, H. C.; Chang, J. *Nat. Commun.* **2017**, *8*, 15573.
- (13) Montoya, S. A.; Tolley, R.; Gilbert, I.; Je, S.-G.; Im, M.-Y.; Fullerton, E. E. *Phys. Rev. B* **2018**, *98*, 104432.
- (14) MacKinnon, C. R.; Lepadatu, S.; Mercer, T.; Bissell, P. R. *Phys. Rev. B* **2020**, *102*, 214408.
- (15) Matsukura, F.; Tokura, Y.; Ohno, H. *Nat. Nanotechnol.* **2015**, *8*, 209–220.
- (16) Hsu, P.-J.; Kubetzka, A.; Finco, A.; Romming, N.; von Bergmann, K.; Wiesendanger, R. *Nat. Nanotechnol.* **2017**, *12*, 123–126.
- (17) Schott, M.; Bernard-Mantel, A.; Ranno, L.; Pizzini, S.; Vogel, J.; Béa, H.; Baraduc, C.; Auffret, S.; Gaudin, G.; Givord, D. *Nano Lett.* **2017**, *17*, 3006–3012.
- (18) Ma, C.; Zhang, X.; Xia, J.; Ezawa, M.; Jiang, W.; Ono, T.; Pircamanayagam, S. N.; Morisako, A.; Zhou, Y.; Liu, X. *Nano Lett.* **2019**, *19*, 353–361.
- (19) Srivastava et al., T. *Nano Lett.* **2018**, *18*, 4871–4877.
- (20) Wang, Y. et al. *Nat. Commun.* **2020**, *11*, 3577.
- (21) Ba, Y. et al. *Nat. Commun.* **2021**, *12*, 322.
- (22) Upadhyaya, P.; Yu, G.; Amiri, P. K.; Wang, K. L. *Phys. Rev. B* **2015**, *92*, 134411.
- (23) Fook, H. T.; Gan, W. L.; Lew, W. S. *Sci. Rep.* **2016**, *6*, 21099.

- (24) Nakatani, Y.; Hayashi, M.; Kanai, S.; Fukami, S.; Ohno, H. *Appl. Phys. Lett.* **2016**, *108*, 1524403.
- (25) Yang, H.; Boulle, O.; Cros, V.; Fert, A.; Chshiev, M. *Sci Rep* **2018**, *8*, 12356.
- (26) Paul, S.; Haldar, S.; von Malottki, S.; Heinze, S. *Nat. Commun.* **2020**, *11*, 4756.
- (27) Paul, S.; Heinze, S. *Phys. Rev. B* **2020**, *101*, 104408.
- (28) <https://www.flapw.de>
- (29) Weinert, M.; Schneider, G.; Podloucky, R.; Redinger, J. *J. Phys.: Condens. Matter* **2009**, *21*, 084201.
- (30) Kurz, P.; Bihlmayer, G.; Hirai, K.; Blügel, S. *Phys. Rev. Lett.* **2001**, *86*, 1106–1109.
- (31) Romming, N.; Pralow, H.; Kubetzka, A.; Hoffmann, M.; von Malottki, S.; Meyer, S.; Dupé, B.; Wiesendanger, R.; von Bergmann, K.; Heinze, S. *Phys. Rev. Lett.* **2018**, *120*, 207201.
- (32) Krönlein, A.; Schmitt, M.; Hoffmann, M.; Kemmer, J.; Seubert, N.; Vogt, M.; Küspert, J.; Böhme, M.; Alonazi, B.; Kügel, J.; Albrithen, H. A.; Bode, M.; Bihlmayer, G.; Blügel, S. *Phys. Rev. Lett.* **2018**, *120*, 207202.
- (33) Spethmann, J.; Meyer, S.; von Bergmann, K.; Wiesendanger, R.; Heinze, S.; Kubetzka, A. *Phys. Rev. Lett.* **2020**, *124*, 227203.
- (34) Hoffmann, M.; Blügel, S. *Phys. Rev. B* **2020**, *101*, 024418.
- (35) Li, W.; Paul, S.; von Bergmann, K.; Heinze, S.; Wiesendanger, R. *Phys. Rev. Lett.* **2020**, *125*, 227205.
- (36) S. Heinze,; K. von Bergmann,; M. Menzel,; J. Brede,; A. Kubetzka,; R. Wiesendanger,; G. Bihlmayer,; S. Blügel, *Nat. Phys.* **2011**, *7*, 713.
- (37) Hardrat, B.; Al-Zubi, A.; Ferriani, P.; Blügel, S.; Bihlmayer, G.; Heinze, S. *Phys. Rev. B* **2009**, *79*, 094411.
- (38) Oba, M.; Nakamura, K.; Akiyama, T.; Ito, T.; Weinert, M.; Freeman, A. J. *Phys. Rev. Lett.* **2015**, *114*, 107202.
- (39) N. Romming,; C. Hanneken,; M. Menzel,; J. E. Bickel,; B. Wolter,; K. von Bergmann,; A. Kubetzka,; R. Wiesendanger, *Science* **2013**, *341*, 636.
- (40) Note that the spin spiral periods obtained at zero magnetic field in the atomistic spin dynamics simulations are consistent with those from the DFT calculations.
- (41) Bessarab, P. F.; Uzdin, V. M.; Jónsson, H. *Comput. Phys. Commun.* **2015**, *196*, 335–347.
- (42) Muckel, F.; von Malottki, S.; Holl, C.; Pestka, B.; Pratzner, M.; Bessarab, P. F.; Heinze, S.; Morgenstern, M. *Nat. Phys.* **2021**,
- (43) Note that for  $K_1 < 0$  the four-site four spin interaction destabilizes skyrmions.<sup>26</sup>
- (44) Note that the four-spin term exhibits the same field dependence for creation and collapse barriers since it has a similar contribution to the FM state as to the skyrmion state.
- (45) Hagemeister, J.; Romming, N.; von Bergmann, K.; Vedmedenko, E. Y.; Wiesendanger, R. *Nat. Commun.* **2015**, *6*, 8455.
- (46) Perdew, J. P.; Burke, K.; Ernzerhof, M. *Phys. Rev. Lett.* **1996**, *77*, 3865–3868.
- (47) Kurz, P.; Förster, F.; Nordström, L.; Bihlmayer, G.; Blügel, S. *Phys. Rev. B* **2004**, *69*, 024415.
- (48) Sandratskii, L. M. *Phys. Status Solidi B* **1986**, *136*, 167.
- (49) Vosko, S. H.; Wilk, L.; Nusair, M. *Can. J. Phys.* **1980**, *58*, 1200–1211.

- (50) Heide, M.; ; Bihlmayer, G.; Blügel, S.  
*Phys. B: Condens. Matter* **2009**, *404*,  
2678.
- (51) H. Mentink, J.; V. Tretyakov, M.; Fasolino, A.; I. Katsnelson, M.; Rasing, T.  
*J. Phys.: Condens. Matter* **2010**, *22*,  
176001.
- (52) F. Bessarab, P.; M. Uzdin, V.; Jónsson, H.  
*Comput. Phys. Commun.* **2015**, *196*, 335–  
347.